Regular Article

ANALYTICAL
AND BIOANALYTICAL
CHEMISTRY
RESEARCH

Published by the
Iranian Chemical Society

***Anal. Bioanal. Chem. Res.**, Vol. 11, No. 3, 309-326, July 2024.*

Simultaneously Removal of Indigo Carmine and Congo Red Anionic Dyes from Aqueous Solutions Using Nickel-Chromium and Zinc-Chromium Layered Double Hydroxides

Bouteiba Ali[a,b,*], Benhadria Naceur[c,d], Ali-Dahmane Tewfik[c,d] and Bettahar Nourredine[a]

[a]*Laboratoire de Chimie des Matériaux Inorganiques et Application (LCMIA), Faculté de Chimie, Université des Sciences et de la Technologie d'Oran (USTO M. B), BP 1505 El M'naouar, 31000 Oran, Algérie*

[b]*Complexe GP1/Z JUMBO, Activité Liquéfaction et Séparation Division (LQS) GNL et GPL, Sonatrach, BP n° 39 Béthioua, Oran, Algérie*

[c]*École Supérieure en Sciences Appliquées, BP 165 RP Bel Horizon ,13000 Tlemcen, Algérie*

[d]*Laboratoire de Chimie des Matériaux L.C.M, Université Oran 1 Ahmed Ben Bella, BP 1524, El-Mnaouer, 31000 Oran, Algérie*

(Received 28 January 2024, Accepted 9 April 2024)

The world is currently grappling with unprecedented levels of water pollution, largely attributed to the presence of detrimental chemicals and dyes posing substantial environmental hazards. This study endeavors to develop highly efficient materials capable of extracting anionic dyes from polluted water reservoirs. Utilizing the coprecipitation method, nickel-chrome and zinc-chrome layered double hydroxides (LDH) were synthesized and subsequently analyzed using advanced analytical techniques. The efficiency of both materials in removing anionic dyes Congo Red (CR) and Indigo Carmine (IC) was investigated by analyzing various parameters, including initial solution pH, adsorbent dose, dye concentration, time, and temperature effects. In binary solutions, ZnCr-LDH exhibited a higher adsorption capacity of 109.10 mg g^{-1} and 78.64 mg g^{-1} for IC and CR dyes, respectively. The competitive removal of a binary dye mixture is primarily influenced by electrostatic attraction. Isotherm models were employed for analysis, with the Freundlich model found to be the best fit for IC adsorption onto NiCr-LDH and the Sips model for IC adsorption onto ZnCr-LDH. In binary systems, the extended Freundlich and non-modified Redlich-Peterson models provided the best fit to the isotherm data. ZnCr-LDH demonstrated higher removal efficiency than NiCr-LDH. Furthermore, both LDH materials exhibited stability and maintained their activity over four successive cycles.

Keywords: Layered double hydroxides, Anionic dyes, Multicomponent system, Competitive adsorption, Isotherms models

INTRODUCTION

The growing global apprehension over pollution stemming from organic dyes originating from various sources is becoming increasingly pronounced. When these pollutants are discharged into the environment without adequate treatment, they present significant hazards to both human health and aquatic ecosystems [1,2]. Synthetic dye molecules, known for their stable and non-biodegradable aromatic structure, frequently demonstrate elevated levels of toxicity, mutagenicity, and carcinogenicity [3]. Hence, it is crucial to mitigate their effects before their release into the environment. The adsorption process stands out as one of the most dependable and commonly utilized methods for purifying waters contaminated with dyes. This method proves to be economically feasible, highly efficient, and operationally straightforward. By utilizing various adsorbents such as activated carbon, fly ash, chitosan, zeolites, and clays, the adsorption process offers an effective solution for removing dyes from wastewater. Its simplicity and effectiveness make it a preferred choice for wastewater

*Corresponding author. E-mail: ali.bouteiba@univ-usto.dz

treatment facilities and industries worldwide. Furthermore, ongoing research efforts aim to improve adsorption techniques, develop novel adsorbents, and optimize process parameters to address the growing challenges of dye pollution in water bodies. Consequently, the adsorption process has emerged as an effective method for dye removal, utilizing various adsorbents such as activated carbon [4], fly ash [5], chitosan [6], zeolites [7], and clays [8-10].

Layered double hydroxides (LDHs), known as anionic clays, are recognized as efficient adsorbents due to their low-cost materials, ease of contaminant separation with high adsorption capacity, and anion exchange properties [11]. LDH materials are formulated as $[M_{1-x}^{2+} M_x^{3+} (OH)_2]^{x+} (A^{n-})_{x/n} \cdot mH_2O$, where M^{2+} and M^{3+} are divalent and trivalent metal cations (Ni^{2+}, Cr^{3+}), A^{n-} is interlayer exchangeable anions such as NO_3^-, CO_3^{2-}, *etc*., and *m* is the number of water molecules [12]. The chemical modification of LDHs can be controlled by varying the metal cations and interlayer anions during co-precipitation [13]. In addition to their high anion exchange properties, LDH materials find applications in various fields such as adsorbents [14,15], catalysts [16], supports [17,18], drug carriers [19], and additives in polymer synthesis [20]. Numerous studies on dye removal have been conducted using LDHs in both single and binary dye solutions. LDH materials have been extensively utilized for the removal of various types of dyes, including crystal violet, methyl orange, orange II, indigo carmine, malachite green, and rhodamine B [21-28]. Heterojunction nanocomposites of MCr-LDHs/BiOBr (M = Zn, Ni, Cu) were synthesized, demonstrating superior photocatalytic degradation of organic pollutants compared to pristine LDHs and BiOBr [29]. Metal-oxide-based LDH nano-hybrids, such as Fe_3O_4/ZnCr-LDH, exhibited a high sorption capacity for removing MO dye from wastewater [30]. Furthermore, GO/NiCr-LDH and GO/NiAl-LDH nanocomposites showed enhanced MO dye removal, while starch NiFe-LDH demonstrated the maximum sorption capacity for MO dye [31-33]. ZnCr-LDH demonstrated dual functionality as both an adsorbent and photocatalyst, facilitating the degradation of AO7 through adsorption and photocatalytic processes [34]. ZnCr LDH also exhibited high photocatalytic activity for visible light-induced oxygen generation, surpassing the efficiency of WO_3 [35].

In this investigation, we produced and evaluated two anionic clays, NiCr-LDH and ZnCr-LDH, to gauge their efficiency in selectively adsorbing binary organic dyes like Congo Red (CR) and Indigo Carmine (IC). We conducted comprehensive explorations of various adsorption parameters, encompassing contact duration, adsorbent quantity, initial dye concentration, and solution pH, to gain a thorough understanding of the adsorption mechanism. Additionally, we employed diverse adsorption isotherms and kinetic models to glean insights into the unique facets of this inquiry.

MATERIALS AND METHODS

The LDH synthesis involved the use of several chemicals, including zinc chloride hexahydrate ($ZnCl_2.6H_2O$, 99%), nickel chloride hexahydrate ($NiCl_2.6H_2O$, 99%), chromium chloride hexahydrate ($CrCl_3.6H_2O$, 99%), sodium hydroxide (NaOH, 99%), sodium carbonate (Na_2CO_3, 99%), sodium chloride (NaCl, 99%), and hydrochloric acid (HCl, 36%). Additionally, anionic dyes, Congo Red diazo (CR) and Indigo Carmine (IC) were used. All chemical reagents were supplied by Sigma Aldrich and used as received.

Synthesis of LDHs

NiCr-LDH and ZnCr-LDH adsorbents were synthesized via the co-precipitation method at ambient temperature. For the preparation of ZnCr-LDH, a solution comprising 0.2 mol $ZnCl_2 \cdot 6H_2O$ and 0.1 mol $CrCl_3 \cdot 6H_2O$ was gradually added to a mixture of 0.2 mol Na_2CO_3 and 0.1 mol NaOH. The pH was maintained at 9 using 1 M NaOH, and the mixture was allowed to age at 80 °C for 24 h. Subsequently, the resultant product was separated through centrifugation, washed, dried at 65 °C for 24 h, and finely ground using an agate mortar. The same procedure was employed for the synthesis of NiCr-LDH.

Instruments Used in Characterization

The materials underwent several characterization techniques, including X-ray diffraction (XRD) using a Bruker D8 Advance diffractometer with CuKα radiation, Fourier transform infrared (FTIR) spectra recorded with a Tensor 27 spectrometer from Bruker Optic GmbH, BET analysis using N_2 gas adsorption-desorption at 77 K, scanning electron microscopy (SEM) on Quanta 250, and

thermogravimetric analysis (TGA) curves obtained using an apparatus equipped with Mettler balances with an accuracy of ±0.1. Additionally, the pHpzc (potential of zero charges) and surface charge properties of LDHs were determined through the pH drift method as described in reference [11].

Adsorption Experiment

In experiments related to adsorption, several parameters were adjusted, including the quantity of adsorbent, the pH of the solution, the initial concentration of the dye, the contact time, and the temperature. The amount of adsorbent used ranged from 0.01 to 0.1 g, while each trial consisted of a 20 ml dye solution (with a concentration of 1000 ppm) in a 50 ml sealed bottle. The adsorbent was added to the solution, which was then agitated for 24 h at room temperature (250 rpm). The suspension was then subjected to centrifugation, and the supernatant was analyzed at regular intervals using UV-visible spectroscopy to determine the remaining concentration of dye. To assess the influence of pH on dye adsorption, pH levels were varied from 2 to 12. A 20 ml dye solution with a concentration of 1000 ppm was prepared, and pH adjustment was performed using 1 N HCl or 1 N NaOH solutions. The optimized amount of adsorbent was added to the solution, and it was left to stand for 24 h. Once the time had elapsed, the suspension was centrifuged, and the supernatant was regularly analyzed using a Shimadzu UV/Vis-1700 spectrophotometer. To study the effects of the initial concentration of the dye in single-dye solutions, concentrations were systematically varied from 50 to 500 ppm. Throughout the study, a consistent adsorption procedure was maintained to ensure uniform conditions and methodology for each concentration point. The same experimental procedure was followed for binary solutions, where the initial dye concentration ratio (IC:CR) was set at 100 ppm:100 ppm. To determine the influence of each dye in the presence of the other, initial concentrations (IC and CR) were systematically varied. IC was adjusted in the range of 100 to 800 ppm while maintaining a fixed concentration of CR (20, 50, 80, and 100 ppm). Additionally, CR was varied in the range of 50 to 500 ppm, while maintaining a fixed concentration of IC (20, 50, 80, and 100 ppm). In each case, the prepared solution was treated with the optimized amount of adsorbent at pH 7, followed by 24 hours of agitation. Subsequently, the suspensions were centrifuged, and the resulting supernatant was analyzed using UV-visible spectroscopy. The adsorbed amount and dye removal percentage were evaluated by [36]

$$Q_{ei} = \frac{(C_{0i} - C_{ei})}{m} \times V \tag{1}$$

$$R\% = \frac{(C_{0i} - C_{ei})}{C_{0i}} \times 100 \tag{2}$$

The chi-square parameter (χ^2) for the best-fitting kinetic model is written as [37,38]:

$$\chi^2 = \sum_{i=1}^{N} \frac{(Q_{e\exp} - Q_{ecal})^2}{Q_{ecal}} \tag{3}$$

Desorption Experiment

The adsorbents' durability and performance were tested by exposing them to repeated cycles of regeneration and reuse in the desorption experiments. Because both dyes had a strong attraction to the methanol solvent, pure methanol (99%) was used to remove the dye molecules from the adsorbent surface. The remaining LDH (after the initial adsorption cycle) was introduced into 20 ml of methanol solvent in this process. The LDH particles in the methanol were allowed to age, followed by several washes with methanol and water to remove any remaining traces of methanol after regeneration. After that, the powders were separated through centrifugation and then dried at 65 °C overnight. This regenerated LDH sample was utilized for up to four adsorption-desorption cycles.

Adsorption Equilibrium Isotherms

To explore the adsorption mechanism, we utilized four established isotherms to establish a relationship between the adsorption behaviors of the dyes on our LDHs. These isotherms include both single-component and multi-component equilibrium models, and their representations are outlined in Tables S1 and S2.
It is worth noting that the constants required for these isotherm models were obtained using a non-linear regression method, using the MATLAB software package. This approach was used to allow for a detailed examination of the adsorption process and to accurately predict the unknown

parameters.

The experiments were meticulously conducted under controlled conditions. This involved using an optimized quantity of LDH, which was either 50 or 70 mg. The volume of the solution (V) was fixed at 20 ml, the pH level was maintained at 7, and the temperature was kept at a consistent 25 °C. The experiments were carried out using a dye concentration of 100 ppm in a single system. In addition, binary solutions were prepared with two specific concentration ratios: 100 ppm initial concentration for one dye and 50 ppm for the other, and 100 ppm initial concentration for both dyes. Each adsorption experiment was allowed to progress for 24 h, facilitated by continuous shaking at a rate of 150 tr/min.

Kinetics Study in Single and Binary Dye Systems

The adsorption kinetics were examined using pseudo-first-order, pseudo-second-order, and intra-particle diffusion models to gain insights into the dynamics of the adsorption process.

Pseudo-first Order Model

The pseudo-first-order kinetic model is often used to describe the adsorption process in various chemical and environmental systems, including the adsorption of dyes onto adsorbent materials like LDHs. This model is used to approximate the kinetics of adsorption reactions when it appears that the rate of adsorption is primarily dependent on the concentration of the solute (dye) in the solution.

The linear form of the pseudo-first-order kinetic model, as mentioned in your question, is expressed as [39]:

$$\ln(Q_e - Q_{et}) = \ln(Q_e) - k_1 t \tag{18}$$

The rate constant k_1 can be determined by linear regression analysis of experimental data, specifically by plotting $\ln(Q_e - Q_t)$ against time t and calculating the slope of the resulting straight line. The value of k_1 represents the apparent rate at which the adsorption process occurs. From the linear plots of $\ln(Q_e - Q_t)$ *versus* t for these adsorption experiments, you can calculate the values of k_1, Q_e, and the determination coefficients for each set of conditions. These values can provide insights into the kinetics and efficiency of the adsorption process under different experimental conditions.

The determination coefficient (R^2) and the chi-square parameter (χ^2) are both statistical measures used to assess the goodness of fit of a kinetic model to experimental data.

Pseudo-second Order Model

The pseudo-second-order kinetic model is another commonly used model to describe the adsorption process, especially when the adsorption mechanism is not strictly first-order and when it seems that the rate of adsorption is more dependent on the surface coverage or the availability of adsorption sites. This model is particularly suitable for situations where chemisorption may be occurring.

The linear form of the pseudo-second-order kinetic model is expressed as [40]:

$$\frac{t}{Q_{et}} = \frac{1}{k_2 Q_e^2} + \frac{1}{Q_e} t \tag{19}$$

Where:

t is the time.

Q_t is the amount of dye adsorbed at time t.

K_2 (g mg^{-1} min^{-1}) is the rate constant of the pseudo-second-order kinetic model.

Q_e is the equilibrium amount of dye adsorbed.

The rate constant K_2 and Q_e can be determined by linear regression analysis of experimental data, specifically by plotting t/Q_t against time t and calculating the slope of the resulting straight line. The value of K_2 represents the apparent rate at which the adsorption process occurs, and it is often expressed in units of (g mg^{-1} min^{-1}).

The equation for the initial sorption rate h is given by:

$$h = k_2 Q_e^2 \tag{20}$$

This equation tells you that the initial rate of sorption (at the beginning of the adsorption process) is directly proportional to the square of the equilibrium concentration (Q_e) of the adsorbate (dye). It provides a measure of how fast the adsorption process is proceeding at the start.

Then the Eq. (19) becomes:

$$\frac{t}{Q_{et}} = \frac{1}{h} + \frac{1}{Q_e} t \tag{21}$$

Intra-particle Diffusion Model

The intra-particle diffusion model is a concept used to describe and understand the diffusion process of solute molecules from the bulk of a solution into the solid phase, which, in our case, would be the adsorbent material. This model is particularly relevant in the context of adsorption studies.

The diffusion process from the bulk of the solution to the solid phase can be described by the intra-particle diffusion model [11].

$$Q_{et} = k_d\, t^{1/2} + C \tag{22}$$

Where k_d (mg g^{-1} $_{min}{}^{-0.5}$) is the intra-particle diffusion rate constant and C (mg g^{-1}) is a constant calculated the intra-particle parameters can be extracted from the linear form when plotting the amount of a solute adsorbed on the surface (Q_t) *versus* $t^{0,5}$ [40].

The Akaike Information Criterion (AIC)

A comparison of the isotherm models was carried out using the Akaike Information Criterion (AIC). The general form for calculating the AIC and AIC_c is given as [44,45]:

$$AIC = 2\ k - n\ \ln(\frac{SSR}{n-k}) \tag{14}$$

In the case of a small sample size, N/P < 40, the bias adjustment or correction for the AIC should be used. This can be defined as:

$$AIC_c = AIC + \frac{2\ k\ (k+1)}{n-k-1} \tag{15}$$

A preferable method is to determine the relative criterion weights for each model such that the model with the highest value is the one having the most statistical confidence. The information criterion weight for the i^{th} model, W_i, can be calculated as follows:

$$w_i = \frac{\exp(-0{,}5\ \Delta\ AIC_{ci})}{\sum_{i=1}^{R} \exp(-0{,}5\ \Delta\ AIC_{ci})} \tag{16}$$

Where $\Delta AIC_{C(i)}$ represents the difference in information criterion value for the i^{th} model relative to the information criterion value of the best candidate model, the model having the lowest AIC_C value. $\Delta\ AIC_{C(i)}$ is defined as:

$$\Delta\ AIC_c = AIC_c - AIC_{c\ \min} \tag{17}$$

In this section, the experiments were conducted using a consistent amount of LDH (either 50 or 70 mg), a constant volume (V = 20 ml), maintaining a pH of 7, a temperature of 25 °C, and a dye concentration of 100 ppm in the case of single-dye systems. In binary solutions, two different initial concentrations were used: 100 ppm IC paired with 50 ppm CR, and 100 ppm IC paired with 100 ppm CR.

Thermodynamic Study

The study also involved an examination of the impact of temperature and thermodynamic parameters (ΔG°, ΔH°, ΔS°) on the adsorption of IC and CR. These thermodynamic parameters are crucial for gaining a deeper insight into the temperature's influence on the adsorption process, and they help determine whether the processes occur spontaneously. The parameters in question encompass the change in enthalpy (ΔH°), entropy (ΔS°), and Gibbs free energy (ΔG°).

To calculate ΔH°, ΔS°, and ΔG°, the following equations are used [11]:

$$k = \frac{Q_{ei}}{C_{ei}} \tag{23}$$

$$\Delta G^{\circ} = \Delta H^{\circ} - T\,\Delta S^{\circ} \tag{24}$$

$$\log(\frac{1000 \times Q_{ei}}{C_{ei}}) = (-\frac{\Delta H^{\circ}}{2.303\ R\ T}) + (\frac{\Delta S^{\circ}}{2.303\ R}) \tag{25}$$

These parameters play a crucial role in understanding the adsorption process of a material. Let's delve into the details of how these parameters affect adsorption:

The effect of temperature on the adsorption of both dyes on the materials in single and binary solutions is investigated at optimum initial dye concentration ratios IC: CR of 100:0, 0:100, and 100:100 (mg l^{-1}). The removal efficiency for both dyes was studied with increasing temperatures from 298 to 328 K.

RESULTS AND DISCUSSION

Characterizations

The X-ray diffraction patterns of both LDHs are shown in Fig. 1a. It could be seen from Fig. 1a that the XRD patterns of both LDHs demonstrate the formation of LDH as a single phase with well-defined h k l planes (0 0 3), (0 0 6), (1 0 1), (0 1 5), (0 1 8), (1 1 0), and (1 1 3). The diffraction peaks for both materials align with a hexagonal lattice exhibiting rhombohedral 3R symmetry [46]. The unit cell parameters a and c can be determined as a = 2 d_{110} and c = 3 d_{003}. The structural parameters are presented in Table 1, and the obtained results are consistent with those reported for hydrotalcite-like compounds [40].

In the FTIR spectra of both samples (Fig. 1b), characteristic bonds corresponding to the hydrotalcite-like structure with CO_3^{2-} as counter anions are evident. The broad and strong band centered at 3441 cm^{-1} is attributed to interlayer water molecules, while the band at 1620 cm^{-1} corresponds to the deformation mode of H-O-H of interlayer water molecules in LDH [11]. The band at 1359 cm^{-1} is due to the ν_3 mode dealing with interlayer carbonate species [47, 48]. Finally, the vibrational modes in the brucite-type layer are due to Zn-O, Ni-O, Cr-O, and metal-oxygen-metal vibrations which are localized in the range of 500-760 cm^{-1} [18].

TGA analysis was used to look at the thermal behavior of both LDHs. Figure S4 illustrates the three primary weight losses that the LDH materials show: for NiCr-LDH 17% from 50 to 200 °C, 13% from 200 to 380 °C, and 7% from 380 to 1000 °C. ZnCr-LDH showed three weight loss observations: a 17% weight loss from 50 to 200 °C, a 13% weight loss between 200 and 365 °C, and a 4% mass reduction of the material from 365 to 640 °C.

Table 1. Structural Parameters of Both LDHs

Sample	A (Å)	c (Å)	Interlamellar Distance (d_{003}) (Å)
NiCr-LDH	3.04	22.98	7.51
ZnCr-LDH	3.08	22.50	7.50

Both ZnCr-LDH and NiCr-LDH materials lost weight in two stages. The loss of physically adsorbed and interlayer water was responsible for the first stage, while the first step of dihydroxylation and the removal of carbonate ions from the interlayer were responsible for the second. Metal oxides were created during the third weight loss when the LDH underwent dihydroxylation and carbonation reactions [11]. Table 2 provides a summary of the textural properties of these adsorbents, and Fig. S5 depicts the N_2 adsorption-desorption isotherms and pore size distribution, determined using the Barrett-Joyner-Halenda (BJH) method.

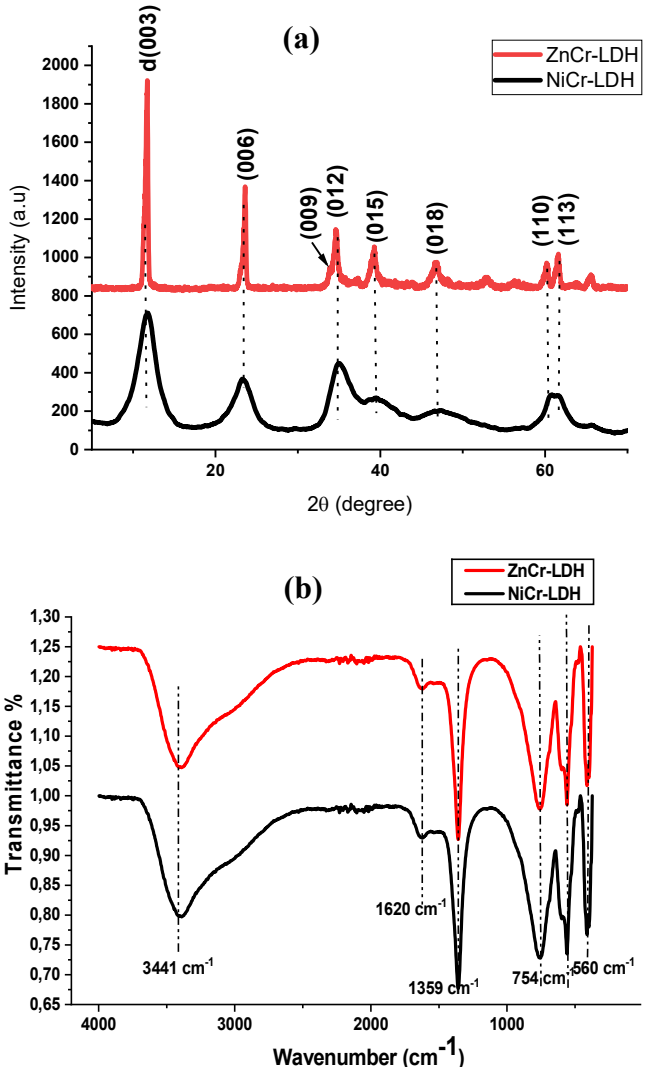

Fig. 1. (a) XRD patterns of NiCr-LDH and ZnCr-LDH (b) FTIR spectra of ZnCr-LDH and NiCr-LDH.

The corresponding isotherms exhibit type IV behavior, indicating mesoporous solids according to IUPAC nomenclature [10]. It is observed that capillary condensation in the pores is not distinctly defined for both materials, suggesting a non-homogeneous pore size distribution. NiCr-LDH (Average pore diameter = 4.107 nm) displays a type H3 hysteresis loop, indicating the formation of mesoporous structures with an irregular agglomeration of plate-like particles and pores wider than approximately 4 nm. Conversely, ZnCr-LDH (Average pore diameter = 3.176 nm) exhibits a completely reversible isotherm, suggesting narrower mesopores [49]. This finding is associated with a surface area approximately 2.25 times greater than that of NiCr-LDH.

The morphological observations of the two LDH compounds are shown in Fig. 2. The ZnCr-LDH particles in

Table 2. Textural Characteristics of the Adsorbents

Adsorbent	BET Surface area (m^{-2} g)	Average pore volume (cm^{-3} g)	Average pore diameter (nm)	Crystallite size (nm)
NiCr-LDH	74.7	0.1	4.107	26.12
ZnCr-LDH	167.825	0.164	3.176	192.94

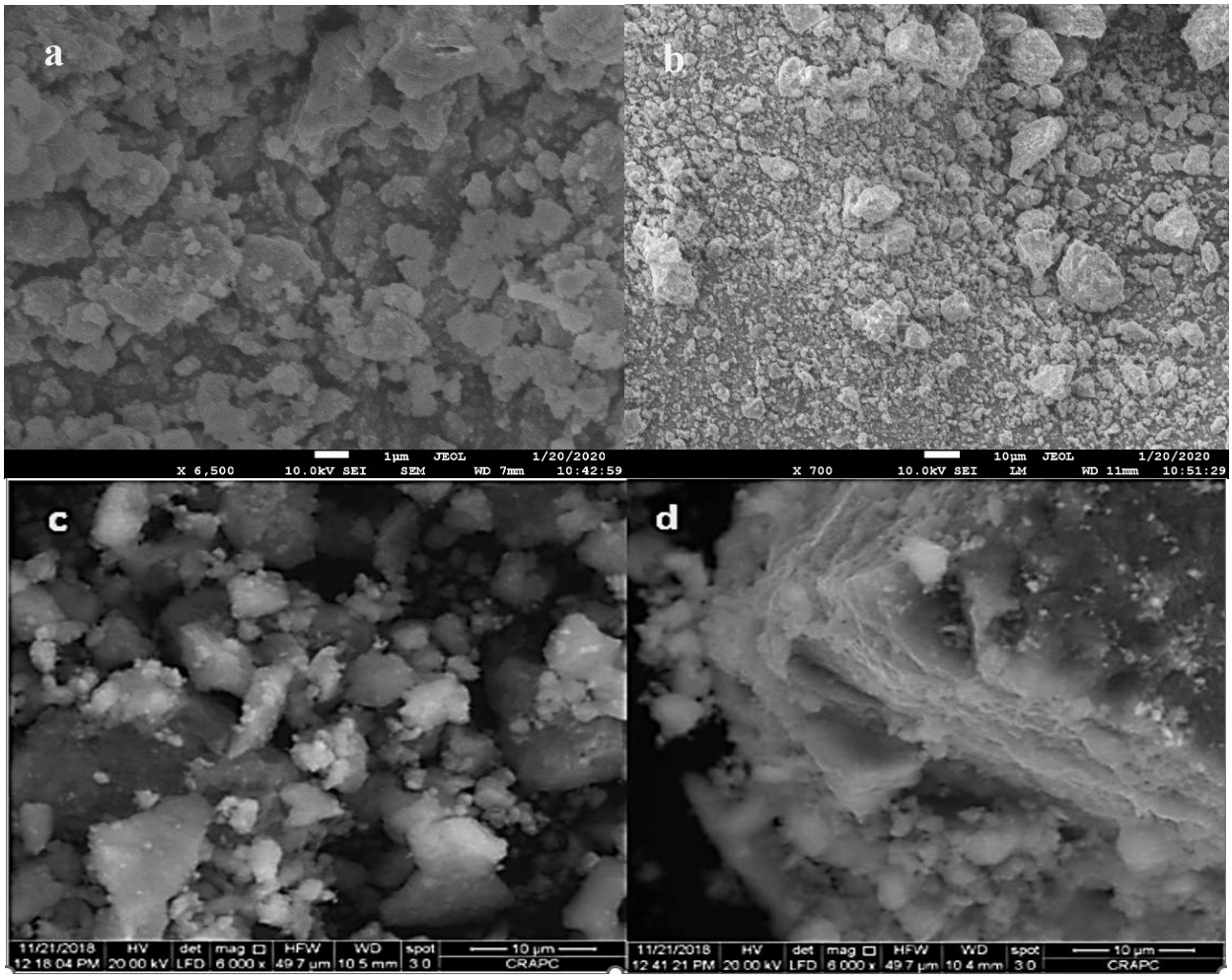

Fig. 2. SEM micrographs of ZnCr-LDH (a, b) and NiCr-LDH (c, d).

Fig. 2a, 2b are unshaped nanoparticles with varying sizes, while the second LDH particles are irregular plate-like particles that have a stacked sheet structure. The ZnCr-LDH particles have a diameter ranging from 1 to 30 µm, and the NiCr-LDH particles have a diameter ranging from 2 to 10 µm, as shown in Fig. 2c, 2d.

ADSORPTION RESULTS

Effect of Adsorbent Amount

In the case of both dyes, it is evident that the quantity of adsorbent significantly influences the adsorption process. As the amount of adsorbent increases, the removal of IC and/or CR dyes also increases (Fig. S6). This outcome can be attributed to the increased availability of adsorption sites on the adsorbent. However, no notable changes in removal efficiency were observed beyond a certain threshold of adsorbent quantity. This can be related to the conglomeration of adsorbent particles, and hence there is no increase in the effective surface area of LDH. Therefore, 0.07 g and 0.05 g were chosen as the optimum doses for NiCr-LDH and ZnCr-LDH, respectively.

Influence of pH on Dye Adsorption

The initial pH of the dye solution plays a pivotal role in determining the adsorption capacity, as depicted in Fig. S7. NiCr-LDH demonstrates optimal and consistent total dye removal within the pH range of 2 to approximately 9.25 in both solution systems. However, an increase in pH beyond 9.25 leads to a decrease in the adsorption capacity. Conversely, for ZnCr-LDH, maximum adsorption is observed within the pH range of 2 to about 10.25, with a subsequent decline in adsorption capacities beyond this value. This behavior is directly linked to the surface charge properties of the LDH material. The point of zero charge (PZC) for our samples is approximately 9.25 for NiCr-LDH and 10.25 for ZnCr-LDH (Fig. S8). In addition to the positive charge resulting from isomorphic substitution, LDH exhibits variable charges due to the adsorption of ions from the solution, such as H^+ or OH^-, depending on the solution's pH and the LDH powders' PZC value [11]. Below the PZC, the LDH external surface carries a positive charge. Furthermore, the negative charge of IC or CR in the solution originates from the SO^{3-} group. At pH 7, strong electrostatic interactions occur between the positively charged LDH surface and dye anions, facilitating their robust adsorption onto the surface. The significant decolorization of dyes at this pH results from the direct interaction of the dye molecule with the adsorbent.

Single Dye Adsorption Isotherms

The experimental equilibrium adsorption data were collected by altering the concentrations of IC or CR while maintaining a constant dosage of LDHs. Figures 3a and b illustrate the experimental adsorption equilibrium data for each dye, plotted with various models.

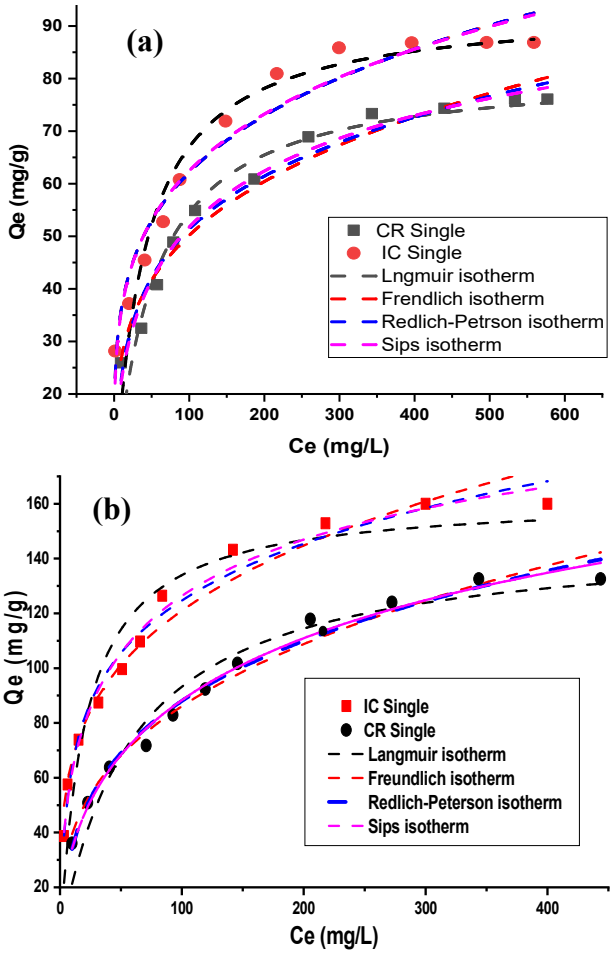

Fig. 3. Isotherm plots for IC and CR adsorption on (a) NiCr-LDH (b) ZnCr-LDH with different models (T = 25 °C, pH = 7 m NiCr-LDH = 0.07 g, m ZnCr-LDH = 0.05 g, V = 20 ml, Time = 24 h).

Table 3 presents the parameters related to dye adsorption using various isotherm models, including the determination coefficient values (R^2), the sum of squares due to errors (SSE), AICs, and Wi, along with the experimental data. It is evident that the regression coefficients obtained from the Freundlich, Redlich-Peterson, and Sips isotherms are

Table 3. The Isotherm Adsorption Models for Single Dye Solution on Both Materials

Isotherm model	Parameters number	Parameters values NiCr-HDL		ZnCr-LDH	
		IC	CR	IC	CR
Langmuir	2	Q_{max} = 93.7 K_L = 0.025 R^2 = 0.83 SSE = 81.37 AIC = 30.22 AIC_C = 29.21 W_i = 1.103E-06	Q_{max} = 81.96 K_L = 50 R^2 = 0.92 SSE = 23.07 AIC = 16.35 AIC_C = 15.34 W_i = 2.51E-04	Q_{max} = 162 K_L = 0.047 R^2 = 0.95 SSE = 20.4 AIC = 15.00 AIC_C = 13.99 W_i = 1.18E-06	Q_{max} = 148.3 K_L = 0.017 R^2 = 0.97 SSE = 9.25 AIC = 6.3 AIC_C = 5.29 W_i = 5.47E-05
Freundlich	2	K_f = 21.44 n_f = 4,3 R^2 = 0.99 SSE = 6.72 AIC = 2.79 AIC_C = 1.77 W_i = 0.99	K_f = 14.62 n_f = 3.7 R^2 = 0.98 SSE = 6.21 AIC = 1.92 AIC_C = 0.90 W_i = 0.34	K_f = 35.11 n_f = 3.863 R^2 = 0.99 SSE = 1.52 AIC = -13.56 AIC_C = -14.58 W_i = 0.19	K_f = 18.22 n_f = 2.966 R^2 = 0.99 SSE = 1.93 AIC = -10.94 AIC_C = -11.95 W_i = 0.30
Redlich–Peterson	3	a = 779.49 b = 68.08 β = 0.67 R^2 = 0.97 SSE = 29.6 AIC = 22.39 AIC_C = 18.08 W_i = 2.87E-04	a = 7.94 b = 0.4 β = 0.781 R^2 = 0.98 SSE = 11.8 AIC = 12.28 AIC_C = 7.98 W_i = 0.01	a = 28.56 b = 0.697 β = 0.766 R^2 = 0.99 SSE = 2.41 AIC = -5.12 AIC_C = -9.51 W_i = 0.015	a = 9.973 b = 0.357 β = 0.730 R^2 = 0.99 SSE = 3.41 AIC = -1.38 AIC_C = -5.69 W_i = 0.0143
Sips	3	Q_{max} = 590.14 K_{Sip} = 2.68 E-6 ms = 0.417 R^2 = 0.94 SSE = 28.7 AIC = 22.05 AIC_C = 17.74 W_i = 3.4E-04	Q_{max} = 121.53 K_{Sip} = 0.006 ms = 0.51 R^2 = 0.98 SSE = 5.53 AIC = 3.94 AIC_C = -0.37 W_i = 0.65	Q_{max} = 165.1 K_{Sip} = 0.039 ms = 1.1 R^2 = 0.99 SSE = 1.17 AIC = -13.15 AIC_C = -17.46 W_i = 0.796	Q_{max} = 262.3 K_{Sip} = 0.003 ms = 0.529 R^2 = 0.99 SSE = 1.7 AIC = -9.04 AIC_C = -13.34 W_i = 0.658

comparable and greater than those from the Langmuir isotherm for both adsorbents. This indicates the heterogeneous adsorption of IC and CR on ZnCr-LDH and NiCr-LDH. The best fitting models for the adsorption of IC onto NiCr-LDH can be classified in the following order: Frendlich > Sips > Redlich-Peterson > Langmuir.

The best-fitting model is the Frendlich model, owing to its higher Wi and lower AICc values. While the Langmuir model with the highest AICc and the lowest W_i values for both materials can't fit well with the adsorption isotherm data for both dyes, for the adsorption of IC onto ZnCr-LDH, the best-fitting model was the Sips model. For CR adsorption on both materials, the Sips model was the best isotherm model. The Langmuir isotherm yielded maximum adsorption capacities of 162 mg g^{-1} and 148.3 mg g^{-1} for IC and CR, respectively, on ZnCr-LDH. For NiCr-LDH, the maximum adsorption capacities were determined to be 93.7 mg g^{-1} for IC and 81.96 mg g^{-1} for CR. As mentioned in Fig. 6b, the adsorption capacity of ZnCr-LDH for IC is higher than that for CR dye. The same result was observed for NiCr-LDH, the adsorption capacity towards IC was 1.4 times greater than that towards CR. This can be explained firstly by the smaller size of IC dye than that of CR molecule, and hence IC can further diffuse into the interlayer of LDH. The high adsorption capacity of ZnCr-LDH compared to that of NiCr-LDH towards both dyes is due to the high surface area of ZnCr-LDH. The adsorption parameters obtained for binary dye adsorption isotherms are given in Table 4. Based on the AICc and W_i values, it can be concluded that the non-modified Langmuir (NL), modified Langmuir (ML), and extended Langmuir multicomponent isotherms (EL) are not appropriate models for fitting the adsorption isotherm data of the dyes in binary systems on both materials.

Binary Dye Adsorption Isotherms

Based on the SSE, R2, AICc, and Wi values, it was determined that the extended Freundlich model was more valid in describing the adsorption of IC dye onto NiCr-LDH. Conversely, the NRP model was identified as the most suitable model for the adsorption of IC and CR on ZnCr-LDH, with the highest Wi values of 5.4 and 2481 times for CR and IC dye, respectively. Additionally, the ES model was identified as the optimal model for the adsorption of CR onto NiCr-LDH.

Effect of Contact Time and Initial Dye Concentration

The results underscore an interesting trend: with increasing initial dye concentration, the adsorption capacity for the dye diminishes. This implies that at higher initial dye concentrations, the adsorbents demonstrate a decreased efficacy in adsorbing the dye molecules efficiently.

For all dyes under investigation, the adsorption process exhibits a gradual increase within a specific time frame. Specifically, in the case of ZnCr-LDH, this increase is observed over 60 min. In contrast, for NiCr-LDH, this incremental adsorption continues for 120 min before reaching an equilibrium state. This dynamic indicates that the adsorption of dyes from the aqueous solution is contingent on the presence of available, unoccupied active sites on the external surface of both adsorbents. Interestingly, the equilibrium time, the point at which the adsorption process stabilizes remains relatively consistent across varying initial dye concentrations. This suggests that the equilibrium state is reached independently of the initial dye concentration, implying that the availability of active sites on the adsorbent's surface plays a more significant role in determining the adsorption rate than the initial concentration of the dye itself. These insights provide valuable information about the kinetics of the adsorption process and the role of active sites in this context. For both LDHs, it is seen that the adsorption process of dyes has been well described with a pseudo-second-order kinetic model with a higher determination coefficient value (R^2). The chi-square parameter χ^2 is smaller than 0.48%. Moreover, the values of $Qe_{(cal)}$, calculated from the pseudo-second-order kinetic model, are very close to the values of $Q_{e(exp)}$.

Both adsorbents exhibit a faster adsorption rate for IC compared to CR in both the single solution and binary system, as indicated by the initial rate constant (h) (Table 5). This phenomenon may be attributed to the smaller size of the Indigo carmine molecule compared to Congo red. In adsorption processes, molecules in a solution are attracted to and adhere to the surface of a solid material, known as the adsorbent. This adherence occurs through various forces, including van der Waals forces and chemical or physical bonding, and plays a crucial role in applications such as wastewater treatment and purification. The process of interest in the intra-particle diffusion model is how molecules

Table 4. The Iotherm Models and their Parameters for Binary Dyes on Both Materials

Isotherm model	Single isotherm parameters	Interaction factors	Parameters values NiCr-LDH		ZnCr-LDH	
			IC	CR	IC	CR
(NL)	4	0	$R^2 = 0.72$ SSE = 89.42 AIC = 28.73 $AIC_C = 30.74$ $W_i = 1.27E-51$	$R^2 = 0.82$ SSE = 82.2 AIC = 24.1 $AIC_C = 26.11$ $W_i = 1.88E-49$	$R^2 = 0.73$ SSE = 89.3 AIC = 28.66 $AIC_C = 30.66$ $W_i = 1.09E-45$	$R^2 = 0.84$ SSE = 77.4 AIC = 20.79 $AIC_C = 22.79$ $W_i = 4.27E-44$
(EL)	0	3	$Q_{max} = 59.7$ $K_{EL(IC)} = 0.0162$ $K_{EL(CR)} = 0.038$ $R^2 = 0.77$ SSE = 67.8 AIC = -186.29 $AIC_C = -181.34$ $W_i = 6.31E-51$	$Q_{max} = 21.49$ $K_{EL(CR)} = 0.61$ $K_{EL(IC)} = 0.72$ $R^2 = 0.87$ SSE = 70.7 AIC = -173.15 $AIC_C = -168.21$ $W_i = 2.91E-50$	$Q_{max} = 109.10$ $K_{EL(IC)} = 0.078$ $K_{EL(CR)} = 0.265$ $R^2 = 0.94$ SSE = 16.41 AIC = -55.43 $AIC_C = -50.49$ $W_i = 4.58E-28$	$Q_{max} = 78.64$ $K_{EL(CR)} = 0.011$ $K_{EL(IC)} = 0.739$ $R^2 = 0.86$ SSE = 33.1 AIC = -16.84 $AIC_C = -11.9$ $W_i = 1.46E-36$
(ML)	4	2	$\eta_{(IC)} = 1.039$ $\eta_{(CR)} = 6.401$ $R^2 = 0.73$ SSE = 70.01 AIC = -163.98 $AIC_C = -160$ $W_i = 1.94E-50$	$\eta_{(CR)} = 1.105$ $\eta_{(IC)} = 0.119$ $R^2 = 0.82$ SSE = 79.64 AIC = -141.85 $AIC_C = -140.9$ $W_i = 8.68E-51$	$\eta_{(IC)} = 1.046$ $\eta_{(CR)} = 2.703$ $R^2 = 0.89$ SSE = 50.3 AIC = 3.12 $AIC_C = 7.11$ $W_i = 4.58E-28$	$\eta_{(CR)} = 1.302$ $\eta_{(IC)} = 0.1102$ $R^2 = 0.90$ SSE = 30.15 AIC = -21.98 $AIC_C = -21.04$ $W_i = 1.46E-36$
(EF)	4	3	$X_{(IC)} = 0.2067$ $Y_{(IC)} = 0.3446$ $Z_{(IC)} = 0.5920$ $R^2 = 0.99$ SSE = 1.09 AIC = -200.68 $AIC_C = -199.75$ $W_i = 0.88$	$X_{(CR)} = 0.411$ $Y_{(CR)} = 0.074$ $Z_{(CR)} = 1.390$ $R^2 = 0.99$ SSE = 1.759 AIC = -180.13 $AIC_C = -179.2$ $W_i = 1.49E-05$	$X_{(IC)} = 0.87$ $Y_{(IC)} = 0.861$ $Z_{(IC)} = 0.935$ $R^2 = 0.99$ SSE = 2.79 AIC = -152.89 $AIC_C = -151.95$ $W_i = 1.43E-40$	$X_{(CR)} = 0.211$ $Y_{(CR)} = 2.017$ $Z_{(CR)} = 0.533$ $R^2 = 0.99$ SSE = 2.18 AIC = -166.46 $AIC_C = -165.52$ $W_i = 1.41E-34$
(NRP)	6	0	$R^2 = 0.99$ SSE = 2.41 AIC = -170.02 $AIC_C = -168.02$ $W_i = 1.84E-08$	$R^2 = 0.89$ SSE = 19.78 AIC = -54.2 $AIC_C = -52.24$ $W_i = 1.93E-32$	$R^2 = 0.99$ SSE = 2.07 AIC = -178.39 $AIC_C = -176.38$ $W_i = 0.99$	$R^2 = 0.99$ SSE = 2.06 AIC = -178.65 $AIC_C = -176.65$ $W_i = 0.87$
(MRP)	6	2	$\eta_{(IC)} = 1.16$ $\eta_{(RC)} = 0.984$ $R^2 = 0.99$ SSE = 2.65 AIC = -158.77 $AIC_C = -154.78$ $W_i = 2.45E-11$	$\eta_{(CR)} = 0.998$ $\eta_{(IC)} = 0.3326$ $R^2 = 0.89$ SSE = 71.86 AIC = 25.79 $AIC_C = 26.73$ $W_i = 1.38E-49$	$\eta_{(IC)} = 1.03$ $\eta_{(RC)} = 0.173$ $R^2 = 0.99$ SSE = 2.45 AIC = -163.08 $AIC_C = -159.09$ $W_i = 1.76E-04$	$\eta_{(CR)} = 0.859$ $\eta_{(IC)} = 0.075$ $R^2 = 0.99$ SSE = 2.37 AIC = -161.86 $AIC_C = -160.92$ $W_i = 3.35E-04$
(ES)	6	0	$R^2 = 0.99$ SSE = 1.74 AIC = -187.94 $AIC_C = -185.9$ $W_i = 1.43E-04$	$R^2 = 0.99$ SSE = 1.39 AIC = -200.29 $AIC_C = -198.28$ $W_i = 0.99$	$R^2 = 0.99$ SSE = 2.53 AIC = -167.35 $AIC_C = -165.34$ $W_i = 3.99E-04$	$R^2 = 0.99$ SSE = 2.21 AIC = -174.79 $AIC_C = -172.78$ $W_i = 0,16$

Table 5. Kinetic Parameters for the Dye Adsorption in Both Systems

	Dye	Experiment	Pseudo-first-order model				Pseudo-second-order model				
		Qe_{Exp} (mg g^{-1})	Qe_{cal} (mg g^{-1})	k_1 (1 min^{-1})	R^2	χ^2	Qe_{cal} (mg g^{-1})	k_2 (g/mg/min)	h (mg/g/min)	R^2	χ^2
NiCr-LDH	IC $_{Single}$	28.18	24.44	0.0294	0.90	0.57	28.82	0.0025	392.41	0.99	0.01
	IC $_{Binary}$[b]	26.64	20.11	0.0278	0.96	2.12	26.95	0.0021	455.61	0.99	0.00
	IC $_{Binary}$[c]	21.71	18.41	0.022	0.98	0.59	23.69	0.0017	568.27	0.99	0.17
		25.93	21.4	0.0264	0.95	0.96	26.04	0.0027	368.58	0.99	0.00
		22.54	16.54	0.0261	0.94	2.18	23.26	0.0026	375.07	0.99	0.02
	CR $_{Binary}$[c]	19.5	15.5	0.0264	0.96	1.03	21.32	0.0023	434.6	0.99	0.16
ZnCr-LDH	IC $_{Single}$[a]	38.7	25.85	0.0589	0.93	6.39	42.19	0.0035	286.3	0.99	0.29
	IC $_{Binary}$[b]	32.67	23.19	0.0586	0.93	3.88	36.23	0.0036	281.5	0.99	0.35
	IC $_{Binary}$[c]	25.1	19.09	0.0576	0.94	1.89	28.17	0.004	250.8	0.99	0.33
	CR $_{Single}$[a]	36.04	25.9	0.053	0.95	3.97	40.16	0.0038	263.87	0.99	0.42
	CR $_{Binary}$[b]	29.87	22.32	0.0603	0.96	2.55	33.89	0.0034	295.09	0.99	0.48
	CR $_{Binary}$[c]	22.91	15.32	0.073	0.95	3.76	25.5	0.0047	209.94	0.99	0.26

[a](100 mg l^{-1}), [b](100:50 mg l^{-1}) and [c](100:100 mg l^{-1}).

move from the bulk of the solution (where they are in higher concentration) into the interior of the solid phase (the adsorbent material). This movement is essential for efficient adsorption. The intra-particle diffusion model focuses on describing how this movement occurs. It suggests that the process is not instantaneous but proceeds in stages. The model assumes that diffusion within the solid particle is a rate-limiting step and that the rate of adsorption is proportional to the square root of time ($t^{0.5}$). This implies that, initially, the rate of adsorption is relatively fast, but it gradually slows down as the adsorbate molecules move deeper into the solid phase.

The adsorption of both dyes onto LDHs in single and binary systems can be well-fitted by the intra-particle diffusion model ($R^2 > 0.997$). The study reveals a two-step mechanism governing the adsorption process, shedding light on the intricacies of this phenomenon. In the first step, molecules undergo diffusion towards the external surface of the adsorbent. This marks the initial phase where molecules embark on their journey from the bulk solution to the solid adsorbent. It's the stage where the interface between the solution and the adsorbent plays a pivotal role in accommodating these molecules.

The second step, which stands as a critical phase, revolves around intra-particle diffusion. Here, molecules navigate within the interior of the adsorbent. This particular step is regarded as rate-limiting, signifying that the pace of adsorption is notably influenced by the way molecules diffuse within the adsorbent material itself. Understanding this intra-particle diffusion is essential for optimizing the efficiency of the adsorption process and gaining insights into the kinetics that underlie this adsorption mechanism. Moreover, the calculated parameters associated with this model are consolidated in Table 6. Among these parameters, k_{d1} and k_{d2} represent specific rate parameters. Notably, the value of k_{d1} surpasses that of k_{d2}. This discrepancy in rate parameters can be attributed to the constraints associated with available vacant sites for diffusion and the phenomenon of pore blockage within the adsorbent material. These insights illuminate the underlying dynamics of the adsorption process and provide valuable information for further investigation and optimization.

Table 6. Kinetic Parameters for Intra-particle Diffusion of IC and CR on LDH

	Intra-particle diffusion model			
	Dye	K_d (mg/g/min$^{0.5}$)	C (mg g^{-1})	R^2
NiCr-LDH	IC $_{Single}$[a]	1.78	9.1	0.99
	IC$_{Binary}$[b]	1.57	4.3	0.99
	IC $_{Binary}$[c]	2.01	5.1	0.99
	CR $_{Single}$ [a]	1.7	7.6	0.99
	CR $_{Binary}$[b]	1.5	6.4	0.99
	CR $_{Binary}$[c]	1.2	6.2	0.99
ZnCr-LDH	IC $_{Single}$[a]	2.9	22.58	0.99
	IC $_{Binary}$[b]	1.49	21.22	0.99
	IC $_{Binary}$[c]	1.69	12.21	0.99
	CR $_{Single}$ [a]	1.95	21.53	0.99
	CR $_{Binary}$[b]	2.04	14.76	0.99
	CR $_{Binary}$[c]	1.76	9.92	0.99

[a](100 mg l^{-1}), [b](100:50 mg l^{-1}) and [c](100:100 mg l^{-1}).

Influence of Temperature and Thermodynamic Parameters

The Gibbs free energy (ΔG°) serves as a fundamental indicator of the spontaneity of a process. In the realm of adsorption, a negative ΔG° value signifies that the process is thermodynamically favorable and spontaneous. Conversely, a positive ΔG° value denotes a non-spontaneous adsorption process. When ΔG° is zero, it signifies that the system is at equilibrium. A lower negative value of ΔG° typically suggests stronger adsorption.

The second thermodynamic parameter is the enthalpy change (ΔH°), which represents the change in heat energy during adsorption. It provides insights into whether the adsorption process is exothermic (ΔH° < 0) or endothermic (ΔH° > 0). Exothermic adsorption releases heat, while endothermic adsorption absorbs heat. Knowledge of ΔH° helps in understanding the energy exchange between the adsorbate and adsorbent, influencing the strength of adsorption.

The change in entropy (ΔS°) is an important parameter directly related to the change in randomness or disorder during adsorption. A positive ΔS° indicates an increase in disorder or randomness, suggesting favorable entropy-driven adsorption. Conversely, a negative ΔS° suggests a decrease in disorder during adsorption. It is essential for understanding the thermodynamic feasibility of the adsorption process.

The temperature changes can significantly impact adsorption. Higher temperatures tend to favor endothermic adsorption processes as they provide the necessary energy for the adsorption to occur, and in the context of exothermic adsorption processes, where heat is released, lower temperatures can facilitate the adsorption process.

Based on the observed ΔH°, ΔS°, and ΔG° values, we can infer the following key insights: The adsorption process is characterized as endothermic (ΔH° > 0), signifying that the interaction between LDH and dye molecules necessitates an external energy input. In practical terms, this implies that the adsorption of IC and CR on LDHs involves the absorption of heat from the surroundings, underscoring the energy-demanding nature of this adsorption process.

Another crucial parameter to consider is the change in entropy. In our experiments, we noted a positive change in entropy (ΔS° > 0), signifying an augmentation in disorder or randomness at the solid/liquid interface as the adsorption progresses. This implies that the adsorption process leads to a greater degree of chaos and disarray, potentially because molecules are distributed in a more random fashion across the adsorbent's surface. This rise in entropy indicates a preference for increased disorder within the overall system during the adsorption process.

The ultimate assessment concerns the change in Gibbs free energy, which exhibits a negative value (ΔG° < 0). This signifies that the adsorption process is not only possible but also spontaneous. A negative ΔG° implies that the adsorption can transpire without any need for external intervention or additional energy input. In essence, the adsorption of IC and CR on LDHs is energetically favorable, indicating that the process can naturally advance without an extra energy infusion [50]. The values of the parameters ΔH°, ΔS°, and ΔG° for both systems are collected in Table 7.

COMPARATIVE STUDY

In the assessment of adsorption capabilities for Indigo Carmine (IC) and Congo Red (CR) dyes across different adsorbents, NiCr-LDH and ZnCr-LDH, synthesized in this

Table 7. Thermodynamic Parameters for Adsorption of Dyes

				ΔG° (Kj mol^{-1})			
		ΔH° (Kj mol^{-1})	ΔS° (Kj mol^{-1} K^{-1})	298 (K)	308 (K)	318 (K)	328 (K)
NiCr-LDH	IC $_{Single}$[a]	16.541	0.62	-168.219	-174.419	-180.619	-186.819
	CR $_{Single}$[a]	4.306	0.103	-26.388	-27.418	-28.448	-29.478
	IC $_{Binary}$[b]	11.158	0.071	-10	-10.71	-11.42	-12.13
	CR $_{Binary}$[b]	4.36	0.07	-16.5	-17.2	-17.9	-18.6
ZnCr-LDH	IC $_{Single}$[a]	94.7	0.48	- 48.34	-55.54	-60.42	-65.30
	CR $_{Single}$[a]	11.24	0.049	-3.589	-4.08	-4.58	-5.08
	IC $_{Binary}$[b]	121.43	0.597	-56.516	-62.48	-68.45	-74.43
	CR $_{Binary}$[b]	10.55	0.043	-2.30	-2.73	-3.16	-3.59

[a](100 mg l^{-1}) and [b](100:100 mg l^{-1}).

Table 8. Comparison of Adsorption Capacity of IC and CR by Different Adsorbents

Absorbent	Dosage (g)	Contact time (min)	Dyes	Adsorption capacity (mg g^{-1})	Ref.
Z-α-F NC	0.15	90	IC_{Binary}	39.86	[51]
$Co(OH)_2$	0.06	40	IC_{Binary}	81.3	[52]
MnFe-LDH	0.03	7	IC_{Binary}	17.85	[53]
IPN-CCh	1.5	24 h	IC_{Binary}	130.5	[54]
CTAB-TiO_2	0.04	200	IC_{Binary}	106.24	[55]
ZnCr-LDH	0.05	60	IC_{Binary}	109.10	This work
NiCr-LDH	0.07	120	IC_{Binary}	59.7	This work
graphene oxide-silica composite	0.05	140	CR_{Binary}	333.33	[56]
MgAl-LDH	0.1	360	CR_{Binary}	332.85	[57]
Fe_3O_4@graphene	0.01	30	CR_{Binary}	33.66	[58]
$CoFe_2O_4$/rGO	0.05	30	CR_{Binary}	104.5	[59]
$MnFe_2O_4$	0.1	30	CR_{Binary}	32.206	[60]
NiCr-LDH	0.07	120	CR_{Binary}	21.49	This work
ZnCr-LDH	0.05	60	CR_{Binary}	78,64	This work

study, exhibit competitive efficacy compared to other reported adsorbents. ZnCr-LDH displays superior adsorption capacities for both IC and CR dyes when compared to Z-α-F NC, MnFe-LDH, $Co(OH)_2$, CTAB-TiO_2, $MnFe_2O_4$, $CoFe_2O_4$/rGO, and NiCr-LDH. Conversely, NiCr-LDH also demonstrates a good performance for IC dye. Variables such as dosage, contact time, and experimental conditions exert influence on the adsorption process, underscoring the necessity of considering diverse parameters when assessing adsorption capacities. Further refinement and exploration of synthesis parameters hold the potential to enhance the effectiveness of these materials in dye removal applications.

ADSORPTION MECHANISM

The XRD patterns of NiCr-LDH and ZnCr-LDH were examined before and after adsorption assays to ascertain whether the dye molecules were successfully intercalated in the interlayer space of the LDHs. As depicted in Fig. 7a, b, the reflection peaks (003) and (006) of LDHs undergo changes before and after the adsorption of IC in the single solution and the binary solution. However, after CR adsorption, the two reflection peaks remain unchanged. This observation suggests that IC was effectively inserted into the LDH interlayer, whereas CR was not effectively intercalated in the LDH interlayer. The shift towards smaller diffraction angles indicates an increase in the interlayer distances d(003), reflecting the intercalation of dye molecules in the inter-foliar space. The values of d_{003} are in the following sequence:

For NiCr-LDH

$d_{003\ (LDH\text{-}IC)}$ (7.79 Å) > $d_{003\ (LDH\text{-}IC+CR)}$ (7.72 Å) > $d_{003\ (LDH\text{-}CR)}$ (7.53 Å) = $d_{003\ (LDH)}$ (7.53 Å).

For ZnCr-LDH

$d_{003\ (LDH\text{-}IC)}$ (7.59 Å) ≈ $d_{003\ (LDH\text{-}IC+CR)}$ (7.586 Å) > $d_{003\ (LDH\text{-}CR)}$ (7.54 Å) = $d_{003\ (LDH)}$ (7.54 Å).

In a single solution, the intercalation of the IC molecule in the interfolliar space is significantly greater than that in a binary system. This is probably due to the competition between the anionic functional groups of the dyes and the carbonate ions (CO^{2-}_3) in the solution to reconstruct the layered structures. The CR dye was not effectively intercalated in the LDH interlayer due to the larger dimension of the molecule.

The FT-IR technique is used to investigate the interactions between the functional groups of the dyes and the layers of adsorbents. As seen in Fig. 8, the FT-IR spectra of the pure LDHs after adsorption of IC and CR in the single and binary systems show the presence of a series of new bands at 1130, 1186, and 1615 cm^{-1}, ascribing to the vibration of C-N, symmetric stretching vibrations of the sulfonic acid group (−SO_3−), and the vibration of –N=N– respectively, in dye molecules. This highlight is attributed to the electrostatic interaction between the anionic functional groups of the dyes and the positively charged surface of NiCr-LDH. Moreover, the strong and sharp absorption bands observed for NiCr-LDH after adsorption, around 500-800 cm^{-1} and 1000-1450 cm^{-1}, suggest that IC and CR dyes have effectively intercalated into the LDH layers.

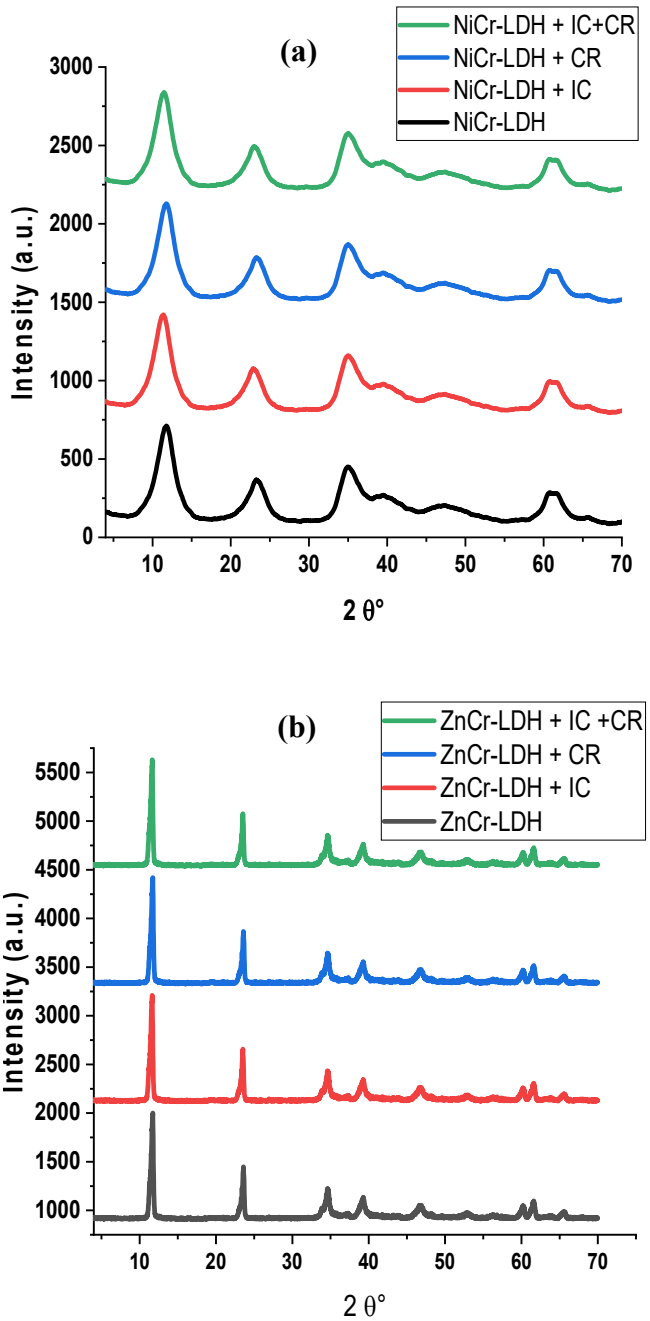

Fig. 4. XRD patterns of (a) NiCr-LDH and (b) ZnCr-LDH before and after adsorption.

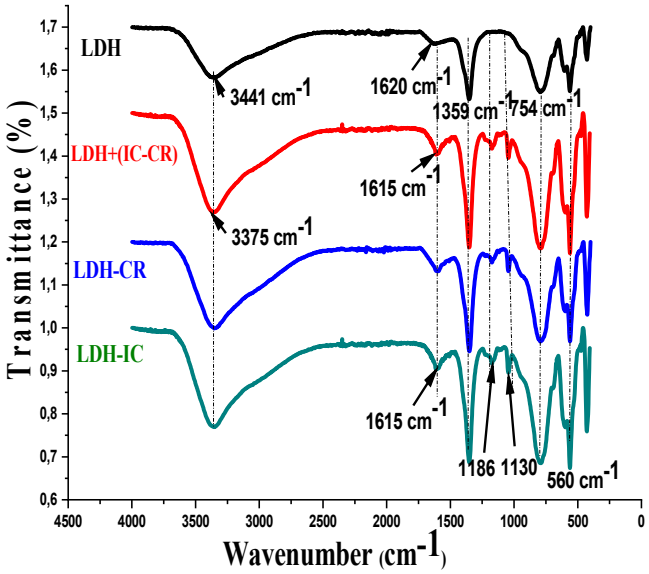

Fig. 5. FT-IR spectra of LDHs after adsorption.

DESORPTION AND REGENERATION

Figure 6 illustrates the adsorption capacity of ZnCr-LDH and NiCr-LDH for two distinct dye types over four consecutive adsorption cycles. The figure demonstrates that both materials maintain their effective adsorption performance for the dyes throughout all four cycles. This indicates the remarkable resilience of ZnCr-LDH and NiCr-LDH, as they exhibit no significant decline in activity during repeated adsorption. Such consistent behavior renders them highly suitable for prolonged and repetitive use in dye removal from aqueous solutions. Overall, these findings present promising implications for the practical application and cost efficiency of these materials in wastewater treatment and purification processes.

CONCLUSION

The study details the synthesis and characterization of NiCr-LDH and ZnCr-LDH materials using the co-precipitation method, which was then employed for dye adsorption in both single and binary systems. XRD patterns confirmed the presence of hydrotalcite-like LDH phases in the synthesized samples. Notably, the surface area of ZnCr-LDH was found to be 2.24 times higher than that of NiCr-LDH. Both materials exhibited a point of zero charge around 10. In terms of adsorption models, the Freundlich and Sips models proved optimal for IC adsorption onto NiCr-LDH and ZnCr-LDH, respectively, while the extended Freundlich and non-modified Redlich-Peterson models best fit both dyes in binary systems.

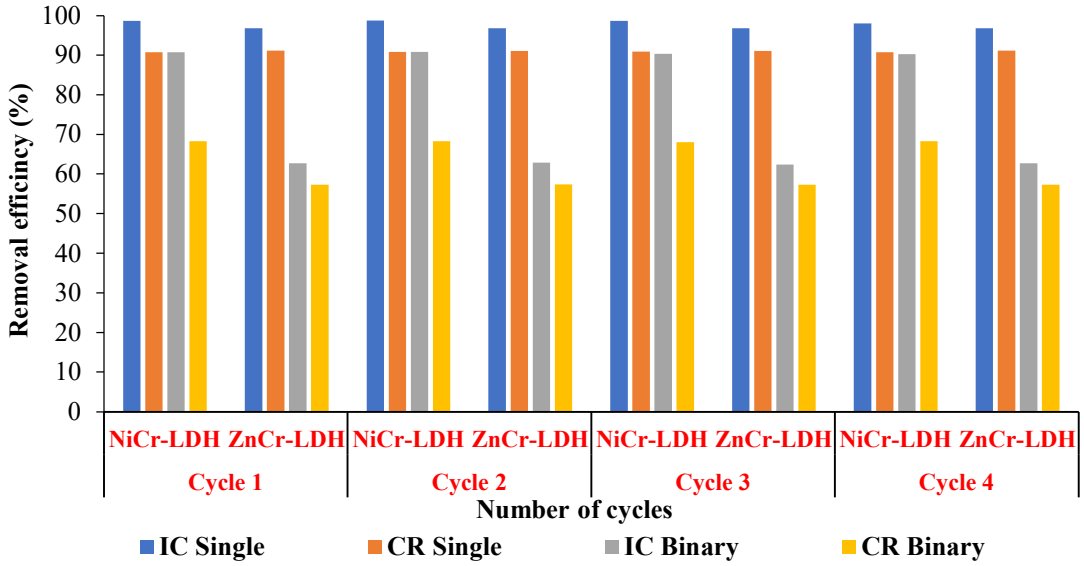

Fig. 6. Adsorption capacity of dye mixture in NiCr-LDH and ZnCr-LDH according to the number of the cycle of washing/adsorption (T = 25 °C, pH = 7 m NiCr-LDH = 0.07 g, m ZnCr-LDH = 0.05 g, V = 20 ml).

ZnCr-LDH demonstrated a superior adsorption capacity compared to NiCr-LDH due to its increased surface area. Kinetic studies revealed a second-order kinetic model, suggesting adsorption occurred through diffusion and the adsorption step. Additionally, the process was found to be endothermic and spontaneous for both materials. LDHs were found to be stable and reusable for multicyclic adsorption processes.

Further analysis revealed that only IC dye was inserted into the LDH interlayer. In discussing analysis methods, the derivative spectrophotometric method was highlighted as a means to simultaneously determine multiple components in mixtures, such as Indigo Carmine (IC) and Congo Red (CR) dyes in a binary system. While offering advantages like simultaneous analysis, enhanced selectivity, sensitivity improvement, and peak resolution, this method is limited in its applicability due to lower reproducibility. It serves as a secondary option when the primary instrumental method is unavailable, but its accuracy in measuring zero-crossing spectra is compromised. Additionally, the resemblance between derivative spectra and zero-order spectra can lead to significant variations in results, particularly when different spectrophotometers are used, resulting in divergent derivatization outcomes.

REFERENCES

[1] J. Sharma, S. Sharma, V. Soni, Reg. Stud. Mar. Sci. 45 (2021).

[2] V. Chandanshive, S. Kadam, N. Rane, B.H. Jeon, J. Jadhav, S. Govindwar. Chemosphere. 252 (2020) 126513.

[3] J. El-gaayda, F. Ezzahra, R. Oukhrib, P. Yap, T. Liu, J. Environ. Chem. Eng. 9 (2021) 106060.

[4] S. Mandal, J. Calderon, S.B. Marpu, M.A. Omary, S.Q. Shi, J. Contam. Hydrol. 243 (2021) 103869.

[5] G. Buema, N. Lupu, H. Chiriac, G. Ciobanu, R. Bucur, D. Bucur, L. Favier, M. Harja, J. Mol. Liq. 333 (2021) 115932.

[6] M. Keshvardoostchokami, M. Majidi, A. Zamani, B. Liu, Carbohydr. Polym. 273 (2021)118625.

[7] T. Cheng, R. Sankaran, P. Loke, C. Wei, B. Liu, W. Siong, Y. Chang, Int. J. Biol. Macromol. 185 (2021) 761.

[8] W. Wang, W. Zhao, H. Zhang, J. Xu, L. Zong, Y. Kang, A. Wang, Powder Technology, 390 (2021) 303.

[9] S.M. Ayisha, V.S. Priya, Agric. Biotechnol. 33 (2021).

[10] A. Bouteiba, N. Benhadria, A. Elaziouti, K. Ezziane, B. Nourredine, Desalin. Water Treat, 201 (2020) 404.

[11] B. Ali, B. Naceur, E. Abdelkader, E. Karima, B. Nourredine, J. Environ. Anal. Chem. 00 (2020) 1.

[12] X. Guo, Y. Ruan, Z. Diao, K. Shih, M. Su, G. Song, J. Clean. Prod. 308 (2021).

[13] T.S. Rad, Z. Ansarian, R.D.C. Soltani, A. Khataee, Y. Orooji, F. Vafaei, J. Hazard. Mater. 399 (2020) 123062.

[14] A.C. Dias, M. Paulo, F. Fontes, Appl. Clay Sci. 191 (2020) 105615.

[15] M. Hasanpour, M. Hatami, Adv. Colloid Interface Sci. 284 (2020) 102247.

[16] F. Rodriguez-rivas, A. Pastor, G. De. Miguel, M. Cruz-yusta, I. Pavlovic, L. Sánchez, Sci. Total Environ. 706 (2020) 136009.

[17] Q. Sun, M. Tang, P. Vang, B. Chen, J. Alloys Compd. 829 (2020) 154552.

[18] B. Ali, E. Abdelkader, B. Naceur, C. Houcined, L. Nadjia, B. Nourredine, J. Environ. Anal. Chem. 1-20 (2021).

[19] S. Sohrabnezhad, Z. Poursafar, A. Asadollahi, Appl. Clay Sci. 190 (2020) 105586.

[20] A.A. Marek, V. Verney, G. Totaro, L. Sisti, A. Celli, N. Bozzi Cionci, D. Di Gioia, L. Massacrier, F. Leroux, Appl. Clay Sci. 188 (2020) 105502.

[21] K. Litefti, M.S. Freire, M. Stitou, González-álvarez, Sci. Rep. (2019) 1.

[22] Z. Wang, L. Zhang, P. Fang, L. Wang, W. Wang, ACS Omega, (2020) 21805.

[23] H. Starukh, S. Levytska, Appl. Clay Sci. 180 (2019) 0-5.

[24] Z. Zhu, M. Xiang, P. Li, L. Shan, P. Zhang, J. Solid State Chem. 288 (2020).

[25] G. George, M.P. Saravanakumar, Environ. Sci. Pollut. Res. 25 (2018) 30236.

[26] Y.S. Aşçı, J. Dispers. Sci. Technol. 38 (2017) 923.

[27] G. Rathee, N. Singh, R. Chandra, ACS Omega. 5 (5) (2020) 2368.

[28] L. EL Mersly, E.M. El Mouchtari, E.M. Moujahid, C. Forano, M. El Haddad, S. Briche, A. Alaoui Tahiri, S. Rafqah, J. Sci.: Adv. Mater. Devices. 6 (2021) 118.

[29] Z. Lü, Y. Cheng, L. Xue, H. Wang, H. Lin, X. Sun, Z. Miao, S. Zhuo, J. Zhou, J. Alloys Compd. 898 (2022) 162871.

[30] D. Chen, Y. Li, J. Zhang, W. Li, J. Zhou, L. Shao, G. Qian, J. Hazard. Mater. 243 (2012) 152.

[31] X. Ruan, Y. Chen, H. Chen, G. Qian, R.L. Frost, J. Chem. Eng. 297 (2016) 295.

[32]Z. Yang, S. Ji, W. Gao, C. Zhang, L. Ren, W. W. Tjiu, Z. Zhang, J. Pan, T. Liu, J. Colloid Interface Sci. 408 (2013) 25.

[33] M. Zubair, N. Jarrah, Ihsanullah, A. Khalid, M.S. Manzar, T.S. Kazeem, A. Mamdouh. Al-Harthi, J. Mol. Liq. 249 (2018) 254.

[34] L. ELMersly, E. E.Mouchtari, E.M. Moujahid, C. Forano, M. El Haddad, S. Briche, A.A. Tahiri, S. Rafqah, J. Sci.: Adv. Mater. 6 (2021) 118.

[35] C.G. Silva, Y. Bouizi, V. Fornés, H. García, J. Am. Chem. Soc. 131, 38 (2009) 13833.

[36] S. Ziane, F. Bessaha, K. Marouf-Khelifa, J. Mol. Liq. 249 (2018) 1245.

[37] M. Imran Khan, A. Shanableh, N. Nasir, S. Shahida, Desalin. Water Treat, 234 (2021) 245.

[38] R.K. Zobon, T.E. Jassim, Mater. Today: Proc, (2021).

[39] J. Pan, Zhou, L.H. Chen, X. Liu, C. Hong, D. Chen, B. Pan, J. Hazard. Mater. 418 (2021) 126300.

[40] P.V. dos Santos Lins, D.C. Henrique, A.H. Ide, C.L. de Paivae Silva Zanta, L. Meili, Environ. Sci. Pollut. Res. 26 (2019) 31804.

[41] S. Kumar, M. Zafar, J.K. Prajapati, S. Kumar, S. Kannepalli, J. Hazard. Mater. 185 (2011) 287.

[42] D.H. Ajay, C.S. Vimal, D.M. Indra, RSC Adv. 75 (2014) 2.

[43] R. Tovar-Gómez, D.A. Rivera-Ramírez, V. Hernández-Montoya, Bonilla-A. Petriciolet, C.J. Durán-Valle, M. A. Montes-Morán, J. Hazard. Mater. (2012) 290.

[44] O.M. Akpa, E.I. Unuabonah, Desalination 272 (2011).

[45] M.H. El-Naas, M.A. Alhaija, S. Al-Zuhair, Environ. Sci. Pollut. Res. 24 (2017) 7511.

[46] R. Benhiti, A. Ait Ichou, A. Zaghloul, G. Carja, M. Zerbet, F. Sinan, M. Chiban, Nanotechnol. Environ. Eng. 6 (2021) 1.

[47] C. Wan, Z. Shi, M. Huang, J. Pan, R. Luo, D. Li, L. Jiang, Int. J. Hydrog. Energy. 46 (2021) 3833.

[48] F. Kefif, K. Ezziane, A. Bahmani, N. Bettahar, S. Mayouf, Bull. Mater. Sci. 42 (2019).

[49] M. Thommes, K. Kaneko, A.V. Neimark, J.P. Olivier, F. Rodriguez-Reinoso, J. Rouquerol, S. Kenneth, W. Sing, Pure Appl. Chem. 87 (2015) 1051.

[50] S. Sharma, G. Sharma, A. Kumar, P. Dhiman, T.S. AlGarni, M. Naushad, J. Sep. Purif. Technol. 278 (2022) 119481.

[51] G. John, N. Abdus-Salam, I.H. Adegoke, J.R. Njimou, E.J. Akor, I.D. Etong, T.C. Bankim, Chemistry Africa. 6 (2023) 1305.

[52] J. Zolgharnein, M. Rastgordani, J. Mol. Liq. 262 (2018) 405.

[53] R. Khalili, M. Ghaedi, M. Parvinnia, M.M. Sabzehmeidani, Surfaces and Interfaces. 23 (2021) 100976.

[54] S. Emik, S. Işık, E.Yıldırım, J. Polym. Environ. 29 (2021) 1963.

[55] J. Zolgharnein, M. Bagtash, N. Asanjarani, J. Environ. Chem. Eng. 2 (2014) 988.

[56] E. Mahmoudi, S. Azizkhani, A.W. Mohammad, L. Yong, A. Benamor, W. Lun Ang, M. Ba-Abbad, J. Environ. Sci. 98 (2020) 151.

[57] Y. Huang, W. Yin, T.L. Zhao, M. Liu, Q.Z. Yao, G.T. Zhou, Nanomaterials 13 (2023) 1145.

[58] Y. Yaoa, S. Miaoa, S. Liub, L.P. Mab, H. Sunb, S. Wangb, J. Chem. Eng. 184 (2012) 326.

[59] W. Yin, S. Haoab, H. Cao, RSC Adv. 7 (2017) 4062.

[60] L. Yang, Y. Zhang, X. Liu, X. Jiang, Z. Zhang, T. Zhang, L. Zhang, J. Chem. Eng. 246 (2014) 88.